IEEE Access
Multidisciplinary | Rapid Review | Open Access Journal

Received January 25, 2021, accepted January 30, 2021, date of publication February 3, 2021, date of current version February 10, 2021.

Digital Object Identifier 10.1109/ACCESS.2021.3056873

Research on Prediction Model of Mining Subsidence in Thick Unconsolidated Layer Mining Area

SHENSHEN CHI[1,2,3], LEI WANG[3], XUEXIANG YU[3], XINJIAN FANG[3], AND CHUANG JIANG[2]

[1]State Key Laboratory of Mining Response and Disaster Prevention and Control in Deep Coal Mines, Anhui University of Science and Technology, Huainan 232001, China
[2]School of Earth and Environment, Anhui University of Science and Technology, Huainan 232001, China
[3]School of Geomatics, Anhui University of Science and Technology, Huainan 232001, China

Corresponding authors: Lei Wang (lwang@aust.edu.cn) and Xuexiang Yu (xxyu@aust.edu.cn)

This work was supported in part by the National Natural Science Foundation of China under Grant 52074010 and Grant 41474026, and in part by the Natural Science Foundation of Anhui Province under Grant 2008085MD114 and Grant 2008085QD178.

ABSTRACT Accurately forecasting the scope of coal mining subsidence area is of great significance to the protection of surface structures. Due to the peculiarities of the unconsolidated layers rock formation, the surface movement of the thick unconsolidated layers mining area converges slowly at the boundary of the basin, and the boundary of the subsidence basin is larger than under conventional conditions. It is found that the existing models have a poor prediction effect at the boundary, and the predicted subsidence basin range is smaller than the actual basin range. To solve this problem, a new surface deformation prediction model based on Boltzmann function (IB) is proposed in this paper. Aiming at the problem that the model function is highly nonlinear and difficult to obtain parameters, the multi-population genetic algorithm (MPGA) is introduced into the parameter solution of the prediction model, and the parameter calculation model based on multi-population genetic algorithm (MPGAIB) is constructed. The simulation experiment and engineering example analysis show that both the overall fitting effect and the fitting effect at the boundary of IB model are closer to the actual situation, The MPGAIB model has good ability to anti-random error and gross error, and the result is stable.

INDEX TERMS Mining subsidence, parameter calculation, probability integral method, prediction model, thick unconsolidated layers.

LIST OF ABBREVIATIONS

IB	Improved Boltzmann function
MPGA	Multi-population genetic algorithm
MPGAIB	Multi-population genetic algorithm parameter model
PIM	Probability integral method
SIE	Semi-infinitive Extraction
FE	Finite Extraction
FEAS	Finite extraction along strike
FEAD	Finite extraction along dip
NUM	The number of populations
LNUM	The number of individuals in each population
GGAP	The generation gap
NVAR	The dimension of the variable
P_c	The crossover probability
P_m	The mutation probability
MAXGEN	The optimal individual maintains the least algebra
RMSE	Root Mean Squared Error
MAE	Mean Absolute Error
AE	Absolute error.

The associate editor coordinating the review of this manuscript and approving it for publication was Sun Junwei.

I. INTRODUCTION

Surface deformation caused by underground mining is a global problem, which will cause damage to surface buildings, railways, rivers, etc., which seriously threatens the normal production and life of the residents in the mining area [1]–[5]. Accurate prediction of surface deformation can not only guide the mining of coal resources, but also provide technical support for the reasonable arrangement of

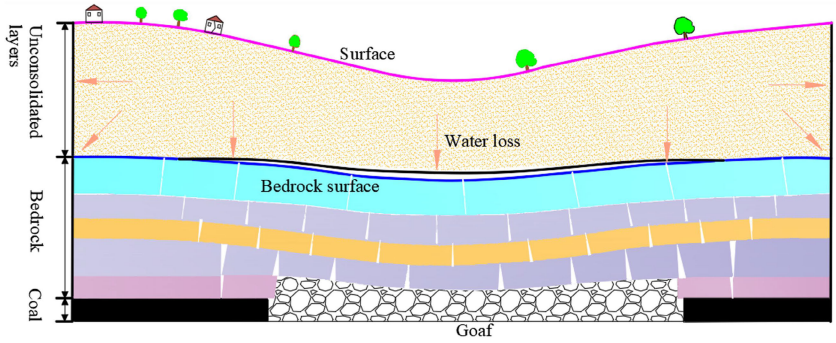

FIGURE 1. Schematic diagram of surface subsidence in thick unconsolidated layers mining area.

the village relocation, restoration and reconstruction of the mining area's ecological environment above the mining area.

The unconsolidated layers are Quaternary and Neogene strata, which are mainly composed of soil, sand, gravel, pebble, etc [6]. It is generally believed that when the thickness of the unconsolidated layer exceeds 50 m, it is called a thick unconsolidated layer [7]. Compared with the conventional mining conditions, the mining subsidence mechanism and time-space law of thick unconsolidated layers are quite different, for example, the maximum surface subsidence value is greater than the coal seam thickness, the surface movement range is large, and the surface subsidence is intense during the mining period [8], [9]. It is generally believed that the surface subsidence is composed of two parts: the subsidence caused by the bedrock and the subsidence caused by the unconsolidated layers. The bedrock is relatively hard and its subsidence conforms to the general subsidence law. When there is no unconsolidated layers in the rock layer, it can see from Fig.1, The subsidence basin of the medium bedrock (blue curve). When there is a unconsolidated layers in the rock layer, on the one hand, the unconsolidated layers itself will sink as the bedrock sinks, and on the other hand, as the mining progresses, the moisture in the unconsolidated layers gradually Erosion, when the rock layer is gradually compacted, causes the maximum subsidence value to be greater than the mining thickness, and with the expansion of the basin, it is often manifested as slow boundary convergence.

Literature search shows that the existing surface prediction models can be divided into four categories, the first category is mainly empirical methods based on measured data, such as the typical curve method, profile function method, etc [10]–[12]. Although this method is simple to operate and has high prediction accuracy, it requires a lot of measured data to build a model, and the model is built for a specific mining area and cannot be used in other mining areas [13], [14].The second type are the influence function method. In mining subsidence, scholars have proposed a variety of influence functions, such as generalized influence function, Probability integral method (PIM) and its improved model, and n-k-g based influence function, etc [15]. Among them, the most commonly used is the PIM model, The PIM

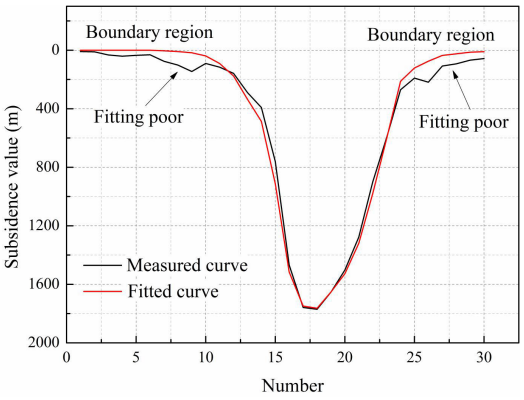

FIGURE 2. Fitting map of subsidence in thick unconsolidated layers mining area.

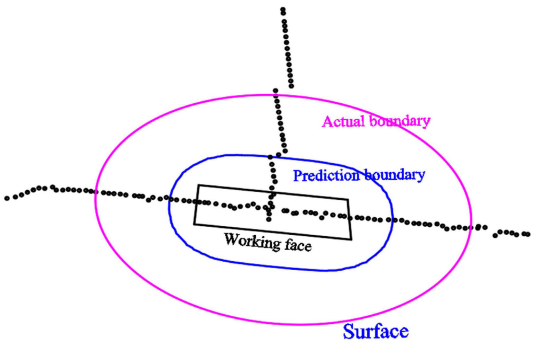

FIGURE 3. Comparison of actual boundary and predicted boundary.

model has the advantages of high prediction accuracy, few parameters, and practical significance of the parameters, but there will be a phenomenon of poor prediction at the boundary shown in Fig.2, and the predicted boundary is smaller than the actual boundary (as shown in Fig.3),Moreover, The PIM function is a highly nonlinear function, and it is difficult to solve the expected parameters. The third category is the method of simulation research, mainly including theoretical model method, numerical simulation method, similar material simulation method [16]–[18]. The advantages of simulation research methods are low cost, short period, intuitive image, etc., but they are currently qualitative researches, and

there are still shortcomings such as unstable similarity and difficult to meet boundary conditions. The fourth category is other prediction methods, such as neural network, time series analysis [19]–[21].This type of model has high prediction accuracy and makes full use of existing data, but this method is often only a single point prediction, and it is difficult to predict the entire subsidence basin.

Due to the above-mentioned special phenomena on the surface of the mining area with thick unconsolidated layers, none of the existing surface prediction models can solve this problem well. In response to the above problem, the author proposed a new prediction model of surface deformation based on the Boltzmann function, and derives the prediction formulas for the main section of the strike, the main section of inclination and any point on the surface. At the same time, comparing the prediction model of PIM, the parameter system of the new model is given. Aiming at the difficult problem of solving the prediction parameters, a model of parameter inversion based on MPGA is proposed.

The rest of the paper is organized as follows: Section II mainly introduces the construction of the prediction model and the method of obtaining the predicted parameters. Sections III and IV conduct simulation experiments and engineering case analysis. Section V is the discussion and Section VI is the conclusion.

II. METHODOLOGY

A. IB MODEL

Boltzmann extended the Maxwell distribution to the Maxwell-Boltzmann distribution. This research result has been widely used. The expression of Boltzmann function is shown in Equation (1). The curve is similar to the prediction formula of the main section along the strike in the semi-infinite mining with PIM. Therefore, the subsidence prediction formula of the main section of the strike based on the Boltmann function can be defined as Equation (2).

$$y = \frac{A_1 - A_2}{1 + e^{(x-x_0)/b}} + A_2 \tag{1}$$

$$w(x) = k\frac{w_0}{1 + \exp(-(x-s)/R)} \tag{2}$$

where k is the proportional factor, w_0 is the maximum subsidence value for the entire mining process, s is the offset of inflection point, and R is the main influence radius.

Differentiating (2), the unit influence function of the Boltzmann function can be calculated as:

$$w_e(x) = dW(x) = \frac{1}{R}\frac{\exp(-x/R)}{(1 + \exp(-x/R))^2} \tag{3}$$

Fig.4 shows the relationship between unit mining subsidence and parameter R. it can be seen from the figure that the smaller R is, the faster the boundary convergence is and the larger the maximum subsidence value is.

In this paper, the surface unit subsidence basin was a combination of two subsidence basins with different parameters R at a certain ratio. Then, the prediction formula of surface

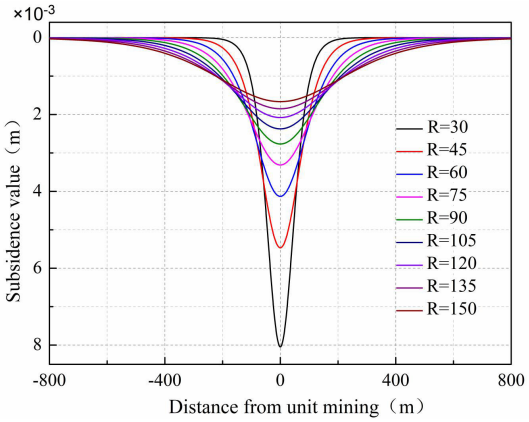

FIGURE 4. Relationship between unit mining subsidence and parameters *R*.

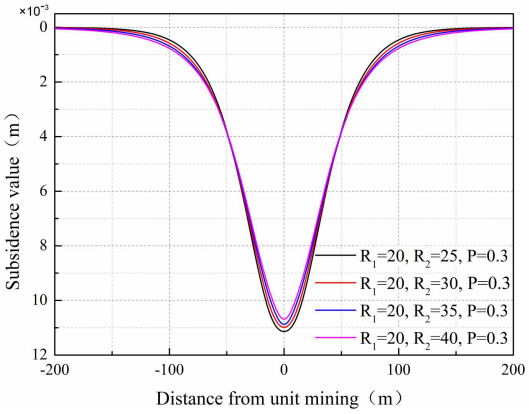

FIGURE 5. Relationship between unit mining subsidence and parameters *R* and *P*.

movement and deformation was established according to the superposition method, as shown in the following:

$$w_e(x) = \frac{1}{R_1}\frac{\exp(-x/R_1)}{(1 + \exp(-x/R_1))^2}(1 - P) + \frac{1}{R_2}\frac{\exp(-x/R_2)}{(1 + \exp(-x/R_2))^2}P \tag{4}$$

where P is the proportional factor.

When $R_1 = 20$, $R_2 = 25$, 30, 35 and 40, $P = 0.3$, the subsidence basin shape of surface unit is shown in Fig.5. It can be seen from Fig.5 that the subsidence model constructed according to a certain proportion combination can better reflect the actual shape of the subsidence basin.

According to the way of coal seam mining, the mining form can be divided into the Semi-infinitive Extraction (SIE) and the Finite Extraction (FE), so the prediction model can be divided into the SIE prediction model and the FE prediction model. Based on the above ideas, this article first derives the SIE surface prediction model, and then derives the strike main section, the dip main section and the surface prediction model at any point under FE conditions. The derivation process is shown in Fig.6. The derivation process is as follows:

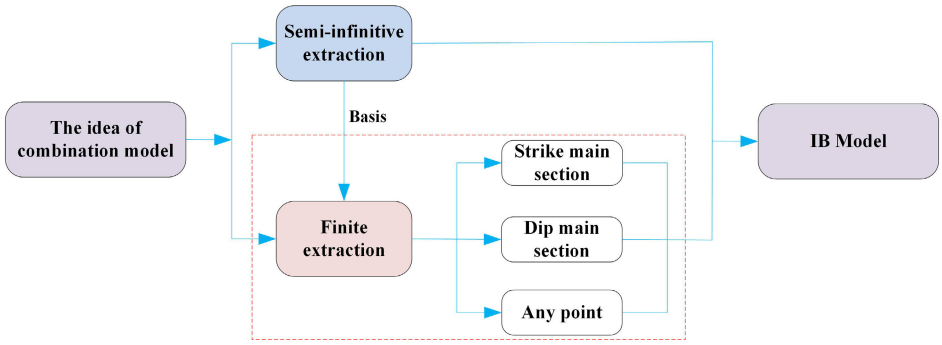

FIGURE 6. The derivation process of the IB model.

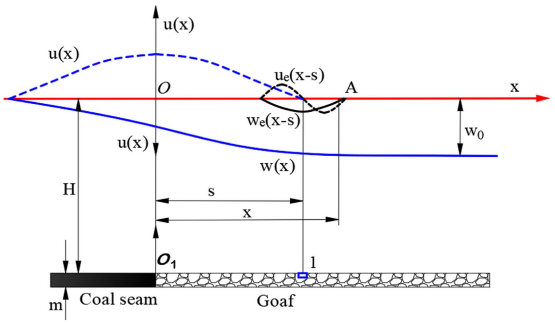

FIGURE 7. Subsidence and horizontal movement of ground surface during SIE.

1) DEFORMATION PREDICTION OF THE MAIN SECTION OF THE BASIN'S STRIKE WHEN SEMI-INFINITIVE EXTRACTION

As shown in Fig.7, SIE means that from the open cut O_1, along the advancing direction of the working face (the right side of the open cut) has been fully mined, and there is no mining on the left side of the open cut, the coordinate system is established with the top of the mining boundary of SIE as the coordinate origin. The positive direction of x-axis points to the direction of goaf, the surface subsidence axis points downward is positive, and the surface horizontal movement axis points upward is positive. The mining thickness of coal seam is m and the mining depth is H. Let the subsidence value of point A with the horizontal axis of s (1 in Fig.7) be $w_e(x-s)$ and the horizontal movement value $u_e(x-s)$ caused by the mining unit.

According to Fig.7 and the above conditions, the subsidence of point A caused by the mining unit with abscissa s should be as follows:

$$dw_e(x) = \frac{1}{R_1}\frac{\exp(-(x-s)/R_1)}{(1+\exp(-(x-s)/R_1))^2}(1-P) + \frac{1}{R_2}\frac{\exp(-(x-s)/R_2)}{(1+\exp(-(x-s)/R_2))^2}Pds \quad (5)$$

In the case of SIE, the boundary is from $s = 0 \rightarrow s = +\infty$,The subsidence of point A can be obtained through integral calculation and simplification:

$$w(x) = \frac{w_0^*(1-P)}{\exp(-x/R_1)+1} + \frac{w_0^* P}{\exp(-x/R_2)+1} \quad (6)$$

According to the PIM derivation experience and knowledge of elastic mechanics, the form of horizontal movement of the unit can be determined, as shown in Equation (7):

$$\begin{aligned} u_e(x) &= B\frac{dw_e(x)}{dx} \\ &= \frac{B^*\exp(-x/R_1)^*(P-1)}{R_1^{2*}(1+\exp(-x/R_1))^2} \\ &\quad - \frac{2^*B^*\exp(-2x/R_1)^*(P-1)}{R_1^{2*}(1+\exp(-x/R_1))^3} \\ &\quad - \frac{B^*\exp(-x/R_2)^*P}{R_2^{2*}(1+\exp(-x/R_2))^2} \\ &\quad + \frac{2^*B^*\exp(-2x/R_2)^*P}{R_2^{2*}(1+\exp(-x/R_2))^3} \end{aligned} \quad (7)$$

where B is a constant.

By the integration of (7), and approximately let:

$$b' = \frac{B}{R_1} = \frac{B}{R_2} \quad (8)$$

The calculation formula for the horizontal movement of the main section along the strike in the SIE can be obtained, as follows:

$$u(x) = bw_0\frac{\exp(-x/R_1)}{(1+\exp(-x/R_1))^2}(1-P) + bw_0\frac{\exp(-x/R_2)}{(1+\exp(-x/R_2))^2}P \quad (9)$$

The slope $i(x)$ is the first derivative of the subsidence $w(x)$, and the formula is as follows:

$$i(x) = \frac{dw(x)}{dx} = \frac{w_0}{R_1}\frac{\exp(-x/R_1)}{(1+\exp(-x/R_1))^2}(1-P) + \frac{w_0}{R_2}\frac{\exp(-x/R_2)}{(1+\exp(-x/R_2))^2}P \quad (10)$$

The curvature k(x) is the first derivative of the slope i(x), and the formula is as follows:

$$\begin{aligned} k(x) &= \frac{di(x)}{dx} \\ &= -\frac{w_0}{R_1^2}\frac{\exp(-x/R_1)[1-\exp(-x/R_1)]^*(1-P)}{(1+\exp(-x/R_1))^3} \\ &\quad - \frac{w_0}{R_2^2}\frac{\exp(-x/R_2)[1-\exp(-x/R_2)]^*P}{(1+\exp(-x/R_2))^3} \end{aligned} \quad (11)$$

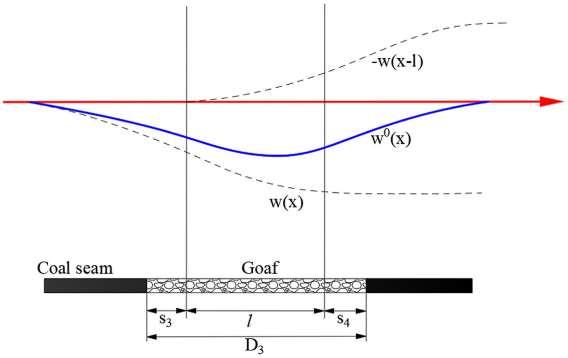

FIGURE 8. Schematic diagram for calculating the deformation of main section along the strike.

The horizontal strain $\varepsilon(x)$ is the first derivative of the horizontal movement $u(x)$, and its formula is as follows:

$$\begin{aligned}\varepsilon(x) &= \frac{du(x)}{dx} \\ &= -b\frac{w_0}{R_1}\frac{\exp(-x/R_1)[1-\exp(-x/R_1)]^*(1-P)}{(1+\exp(-x/R_1))^3} \\ &\quad -b\frac{w_0}{R_2}\frac{\exp(-x/R_2)[1-\exp(-x/R_2)]^*P}{(1+\exp(-x/R_2))^3}\end{aligned} \tag{12}$$

2) DEFORMATION PREDICTION OF THE MAIN SECTION OF THE BASIN'S STRIKE WHEN FINITE EXTRACTION

It is assumed that the coal seam has reached full mining along the inclined direction and hasn't reached full mining along the strike. This situation is called the finite extraction along strike (FEAS) (as shown in Fig.8). The actual mining length along the strike is D_3, and the offset of inflection point is generated due to the cantilever action of the roof. The offset distances of the left and right inflection points were set as s_3 and s_4.

According to the principle of superposition, it can be understood as the difference between two SIE, and the calculation formula of the deformation of the main section along the strike can be obtained as follows:

$$\begin{cases} w^0(x) = w(x) - w(x-l_3) \\ i^0(x) = i(x) - i(x-l_3) \\ k^0(x) = k(x) - k(x-l_3) \\ u^0(x) = u(x) - u(x-l_3) \\ \varepsilon^0(x) = \varepsilon(x) - \varepsilon(x-l_3) \end{cases} \tag{13}$$

where l_3 is the calculated length of strike mining, $l_3 = D_3 - s_3 - s_4$.

3) DEFORMATION PREDICTION OF THE MAIN SECTION OF THE BASIN'S DIP WHEN FINITE EXTRACTION

It is assumed that the coal seam has reached full mining along the strike direction, and is not fully exploited along the inclination. This situation is called finite extraction along dip (FEAD) (as shown in Fig.9). According to the principle of superposition, it can also be understood as the difference between the semi-infinite mining of two coal seams with different depths, and the calculation formula for the movement

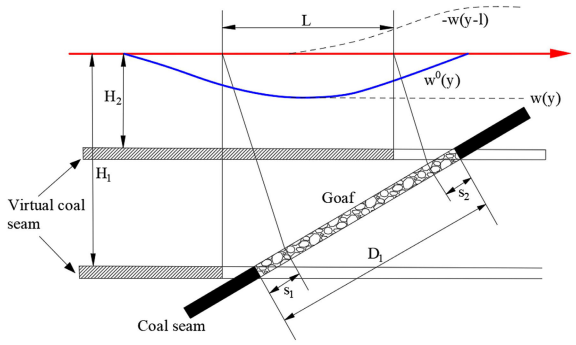

FIGURE 9. Schematic diagram for calculating the deformation of the main section along the inclination.

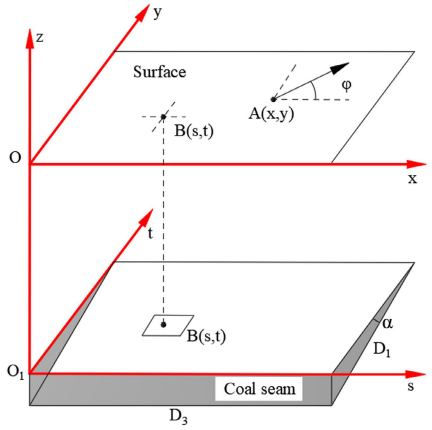

FIGURE 10. Schematic diagram of arbitrary point calculation.

and deformation of the main section along the inclination is as follows:

$$\begin{cases} w^0(y) = w(y) - w(y-l_1) \\ i^0(y) = i(y) - i(y-l_1) \\ k^0(y) = k(y) - k(y-l_1) \\ u^0(y) = [u(y) + w(y)\cot\theta_0] \\ \qquad\quad -[u(y-l_1) + w(y-l_1)\cot\theta_0] \\ \varepsilon^0(x) = [\varepsilon(y) + i(y)\cot\theta_0] \\ \qquad\quad -[\varepsilon(y-l_1) + i(y-l_1)\cot\theta_0] \end{cases} \tag{14}$$

where, l_1 is the calculation length of inclination $l_1 = (D_1 - s_1 - s_2)\sin(\theta_0 + \alpha)/\sin(\theta_0)$, s_1 and s_2 are the offset distances of the inflection point in the direction of downhill and uphill, θ_0 is the propagation angle of extraction, α is the dip angle of coal seam.

4) DEFORMATION PREDICTION OF THE DEFORMATION OF ANY POINT IN A SURFACE MOVING BASIN

As shown in Fig.10, the coal seam is assumed to be a horizontal coal seam. The horizontal projections of the coal seam coordinate system tO_1s and the surface coordinate system xOy coincide. The mining of a unit $B(s, t)$ with a width of ds, a length of dt and a thickness of w_o is conducted at s. Then the mining-induced subsidence value of $A(x, y)$ at any point

on the surface can be expressed as follows:

$$\begin{aligned} dw(x,y) &= w_0 w_e(x-s)\, w_e(y-t) \\ &= w_0\left(\frac{1}{R_1}\frac{\exp(-(x-s)/R_1)}{(1+\exp(-(x-s)/R_1))^2}(1-P)\right. \\ &\quad \left.+\frac{1}{R_2}\frac{\exp(-(x-s)/R_2)}{(1+\exp(-(x-s)/R_2))^2}P\right) \\ &\quad \left(\frac{1}{R_1}\frac{\exp(-(y-t)/R_1)}{(1+\exp(-(y-t)/R_1))^2}(1-P)\right. \\ &\quad \left.+\frac{1}{R_2}\frac{\exp(-(y-t)/R_2)}{(1+\exp(-(y-t)/R_2))^2}P\right) \end{aligned} \tag{15}$$

As shown in Fig.9, if the mining area is O_1CDE, the length of O_1C is D_3, the length of CD is D_1, the subsidence value of point $A(x, y)$ caused by the whole mining can be obtained by (17), as follows:

$$w(x,y) = w_0\int_0^{D_3}\int_0^{D_1} dw(x,y) \tag{16}$$

After simplification, we can get:

$$w(x,y) = \frac{1}{w_0}[w(x) - w(x-D_3)][w(y) - w(y-D_1)] \tag{17}$$

According to the deduction of the prediction formula of the surface deformation of the main section in FEAS and FEAD, the above formula can be converted into:

$$\begin{aligned} w(x,y) &= \frac{1}{w_0}[w(x) - w(x-l_3)][w(y) - w(y-l_1)] \\ &= \frac{1}{w_0}w^0(x)\, w^0(y) \end{aligned} \tag{18}$$

The slope $i(x, y, \varphi)$ of any point $A(x, y)$ on the surface along the φ direction is the derivative of the subsidence $w(x, y)$ in the φ direction.

$$\begin{aligned} i(x,y,\varphi) &= \frac{\partial w(x,y)}{\partial \varphi} \\ &= \frac{\partial w(x,y)}{\partial x}\cos\varphi + \frac{\partial w(x,y)}{\partial y}\sin\varphi \\ &= \frac{1}{w_0}\left[i^0(x)\, w^0(y)\cos\varphi + w^0(x)\, i^0(y)\sin\varphi\right] \end{aligned} \tag{19}$$

Similarly, the curvature formula at any point can be obtained:

$$\begin{aligned} k(x,y,\varphi) &= \frac{\partial i(x,y)}{\partial \varphi} \\ &= \frac{\partial i(x,y)}{\partial x}\cos\varphi + \frac{\partial i(x,y)}{\partial y}\sin\varphi \\ &= \frac{1}{w_0}\left[k^0(x)\, w^0(y)\cos^2\varphi + w^0(x)\, k^0(y)\sin^2\varphi\right. \\ &\quad \left.+i^0(x)\, i^0(y)\sin 2\varphi\right] \end{aligned} \tag{20}$$

The formula for the horizontal movement of any point is as follows:

$$u(x,y,\varphi) = \frac{1}{w_0}\left[u^0(x)\, w^0(y)\cos\varphi + w^0(x)\, u^0(y)\sin\varphi\right] \tag{21}$$

The formula of the horizontal strain at any point can be obtained:

$$\begin{aligned} &\varepsilon(x,y,\varphi) \\ &= \frac{1}{w_0}\left\{\varepsilon^0(x)\, w^0(y)\cos^2\varphi + \varepsilon^0(y)\, w^0(x)\sin^2\varphi\right\} \\ &\quad + \frac{1}{w_0}\left\{\left[u^0(x)\, i^0(y) + i^0(x)\, u^0(y)\right]\sin\varphi\cos\varphi\right\} \end{aligned} \tag{22}$$

5) PARAMETER ANALYSIS

In the IB model, the subsidence factor, the propagation angle of extraction, the offset of inflection point, and the horizontal movement coefficient have the same meaning as defined by the PIM. R_1 and R_2 in the model are important influence radii. The tangent of main influence angle: $\tan\beta_1 = H/4.13R_1$, $\tan\beta_2 = H/4.13R_2$. P is the proportional factor. There are 10 parameters in the new model: q, P, b, θ_0, s_1, s_2, s_3, s_4, $\tan\beta_1$, $\tan\beta_2$.

B. IB PARAMETER CALCULATION

1) MPGA

As shown in the above model expression, the model function is highly nonlinear, so it is difficult to obtain the global optimal solution of the model parameters. Genetic algorithm (GA) is a computational model of biological evolution process which simulates natural selection and genetic mechanism of biological evolution theory. Due to its strong robustness and global search ability, it is widely used in machine learning, pattern recognition, mathematical optimization and other fields. The traditional GA mainly uses a single population for evolution, and the crossover probability and mutation probability are fixed values. Therefore, the premature convergence problem occurs in the application process, which mainly shows that all individuals in the population tend to the same state and stop evolution, and the algorithm cannot get satisfactory solution. In view of the problems of genetic algorithms, MPGA can be used to replace the conventional standard GA in the process of practical application. MPGA introduces the strategy of multi population co evolution, uses immigration operator, and controls the crossover probability and mutation probability in an interval, which effectively avoids the premature convergence problem, At the same time, the essence of the population is introduced to avoid the problem of immature convergence.

2) MPGAIB

This paper introduces the multi-population genetic algorithm into the process of IB model parameter calculation. The solution technical route is shown in Fig.11. The main solution process is as follows:

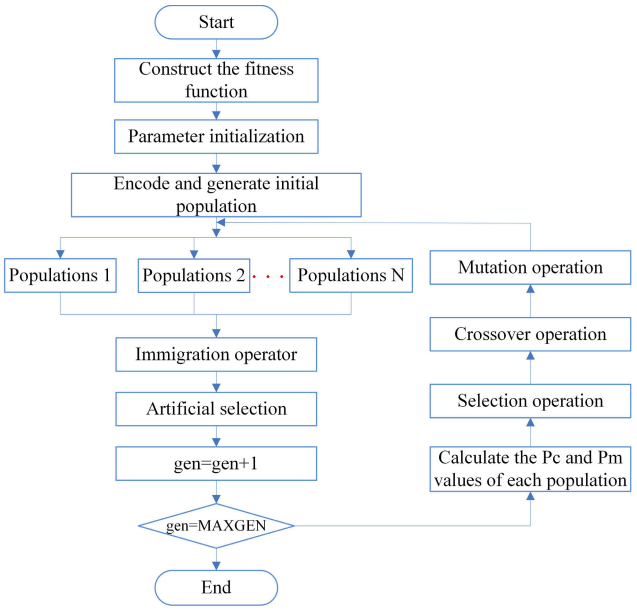

FIGURE 11. The flow chart of parameters inversion.

TABLE 1. Parameters of MPGA.

Parameters	*NUM*	*LNUM*	*GGAP*	*NVAR*
Values	30	100	0.9	10
Parameters	*Pc*	*Pm*	*MAXGEN*	
Values	0.7~0.9	0.001~0.005	100	

(1) Establish the fitness function. Assuming that the measured subsidence and horizontal movement values are W_s and U_s, and the predicted subsidence and horizontal movement values are W_i and U_i, respectively, using the minimum sum of squared differences between the predicted value and the observed value as the criterion, the fitness function is obtained as:

$$f = \sum \left((W_s - W_i)^2 + (U_s - U_i)^2 \right) \tag{23}$$

(2) Setting of MPGA algorithm parameters. It mainly includes the number of populations (*NUM*), the number of individuals in each population (*LNUM*), the generation gap (*GGAP*), the dimension of the variable (*NVAR*), the crossover probability (P_c) and the mutation probability (P_m) of each population, and the optimal individual maintains the least algebra (*MAXGEN*). The specific values are shown in Table 1.

In order to reflect the advantages of the MPGA algorithm, the algorithm needs to use a large crossover probability and a small mutation probability in the early stage of evolution to enhance the global optimization ability, and a smaller crossover probability and a larger mutation probability in the later stage of the evolution to enhance local search ability. According to the range of crossover probability and mutation probability (see Table 1), the adaptive adjustment formula designed in this paper is:

$$P_c = 0.7 + (0.9 - 0.7)^* \text{rand}\,(NUM, 1) \tag{24}$$

$$P_m = 0.001 + (0.05 - 0.001)^* \text{rand}\,(NUM, 1) \tag{25}$$

(3) Coding and population generation. According to the IB parameter range, the binary code corresponding to each parameter is randomly generated based on the binary code to establish the initial population.

(4) Decode, calculate and sort the fitness function value. Calculate the fitness function value of each individual in each population, and sort them from large to small to find the optimal value of each population.

(5) Immigration operation. Perform immigration operations on the optimal value obtained for each population, and replace the worst value of the next population with the optimal value of the previous population in turn.

(6) Artificial selection of elite populations. The best individuals of each species are stored in the elite population to find out the best individuals of the elite population and determine whether the current optimization value is the same as the previous optimization value. If the value is the same, jump to step (8), and if the value is different, do the steps (7).

(7) The crossover probability P_c and mutation probability Pm of each population were calculated, and then the selection, crossover and mutation of each population were performed to generate the new species group and skip to step (3).

(8) Judge whether the *MAXGEN* value meets the set value, if so, decode the output result, if not, skip to step (7) to continue the cycle.

III. SIMULATED EXPERIMENT

A. OVERVIEW OF THE SIMULATED WORKING FACE

Geological and mining conditions of the designed working face are in the following. The mining thickness of the coal seam is 3 m, the dip angle is 3°, the strike length of the coal seam is 600m, the dip length is 300m, and the average mining depth is 500 m. The total caving method is used to manage the roof. The predicted parameters of surface subsidence are as follows: $q = 1$, $P = 0.7$, $b = 0.3$, $\tan\beta_1 = 2$, $\tan\beta_2 = 4$, $s_1 = s_2 = s_3 = s_4 = 45$ m, and $\theta = 85°$. There are 41 monitoring points in the design strike line and 31 monitoring points in the inclination line with a spacing of 30 m. The layout of observation line is shown in Fig.12. According to the geological mining conditions, the predicted parameters of the ground surface and the coordinate values of each monitoring point, the measured subsidence and horizontal movement values of the simulated working face are obtained as shown in Fig.13:

B. RELIABILITY OF MPGAIB

According to the actual measured subsidence of the simulated working face, the MPGAIB parameter model proposed in this paper is used to obtain the fitting parameters. For comparison, the standard genetic algorithm parameter model (GAIB) is used for comparison. Parameter inversion 30 times, the average value of 30 times is used as the final calculated value, and the relative median error (K) and root mean square error (RMSE) of the parameters are calculated as shown in Table 2, and the fluctuation range of the parameters is shown in Fig.14.

TABLE 2. Comparison of stability and accuracy of GAIB and MPGAIB.

Parameters	Design value	GAIB			MPGAIB		
		Average value	K/%	RMSE	Average value	K/%	RMSE
q	1	0.995	0.456	0.008	1	0.033	0.001
P	0.7	0.726	3.659	0.069	0.687	1.911	0.050
b	0.3	0.299	0.066	0.003	0.300	0.013	0.000
θ	85	85.019	0.022	0.108	85.000	0.000	0.006
s_1	45	49.987	11.081	10.877	42.891	4.686	10.733
s_2	45	39.648	11.892	10.868	47.129	4.730	10.862
s_3	45	47.417	5.370	8.845	45.236	0.524	10.478
s_4	45	42.433	5.705	10.485	44.754	0.546	10.423
$\tan\beta_1$	2	2.023	1.172	0.170	2.002	0.097	0.114
$\tan\beta_2$	4	3.895	2.628	0.202	4.034	0.849	0.119

TABLE 3. The results of research on the anti-random error ability of MPGAIB.

Parameters	Design value	W±10 mm、U±3 mm			W±20 mm、U±6 mm			W±30 mm、U±9 mm		
		Average value	AE	K/%	Average value	AE	K/%	Average value	AE	K/%
q	1	1.006	0.006	0.622	1.014	0.014	1.436	1.021	0.021	2.070
P	0.7	0.717	0.017	0.458	0.765	0.065	9.232	0.751	0.051	7.317
b	0.3	0.299	0.001	0.458	0.298	0.002	0.751	0.296	0.004	1.480
θ	85	84.945	0.055	0.064	84.925	0.075	0.088	84.899	0.101	0.118
s_1	45	46.911	1.911	4.248	46.304	1.304	2.897	47.467	2.467	5.483
s_2	45	43.306	1.694	3.764	43.818	1.182	2.626	42.636	2.364	5.253
s_3	45	44.621	0.379	0.841	43.700	1.300	2.889	45.925	0.925	2.056
s_4	45	45.392	0.392	0.872	46.286	1.286	2.859	44.144	0.856	1.903
$\tan\beta_1$	2	1.923	0.077	3.827	1.736	0.264	13.197	1.729	0.271	13.540
$\tan\beta_2$	4	3.960	0.040	0.988	3.870	0.130	3.254	3.891	0.109	2.733

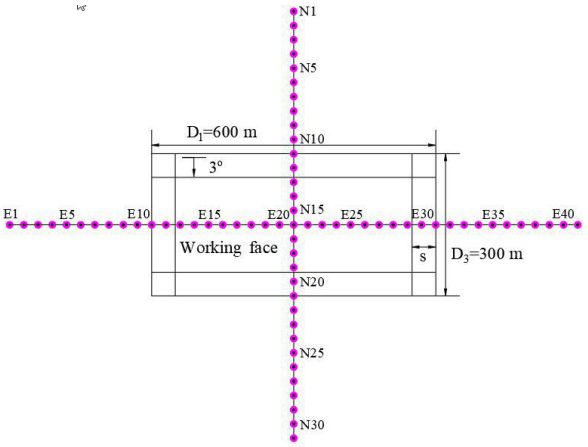

FIGURE 12. Layout of simulated working face.

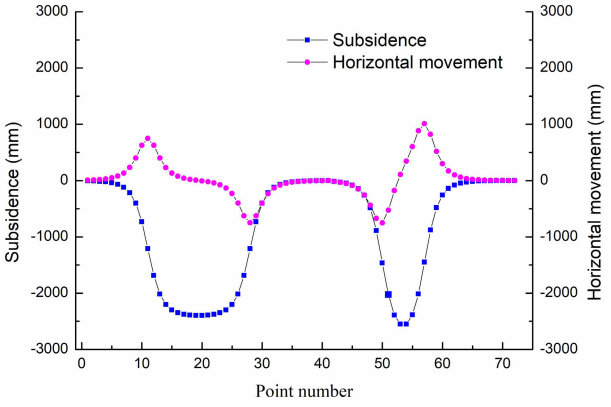

FIGURE 13. Simulate measured subsidence and horizontal movement values.

It can be seen from Table 2 that (1) the maximum K value of the average value of the parameters calculated by GAIB is not more than 11.892%, and the maximum K value of the average parameter value calculated by MPGAIB is not more than 4.730%, which indicates that the MPGAIB model has high accuracy. (2) Except s_3, the RMSE of MPGAIB model is less than GAIB, which indicates that MPGAIB is more reliable than GAIB. It can be seen from Fig.13 that: (1) the parameters q, b, θ, $\tan\beta_1$ and $\tan\beta_2$ calculated by MPGAIB fluctuate near the design value, showing good stability; (2) the numbers of P, s_1, s_2, s_3 and s_4 calculated by the two methods all swing within a certain range, and the fluctuation range is not large.

C. ANTI-RANDOM ERROR ABILITY OF MPGAIB

Due to the influence of complex environment in the field, random error is inevitable in the measurement process. In order to verify whether MPGAIB model has certain anti-interference ability to random error, taking simulated working face as an example, random error of 10,20,40 mm in subsidence values and 3,6,9 mm random error in horizontal movement value were increased respectively, The data with errors are inversed. The specific calculation results are shown in Table.3. Where AE is the absolute error.

It can be seen from Table.3 that with the increase of random error, the error of inversion results increases with the increase of random error, but in general, random error has little influ-

TABLE 4. The results of research on the anti-gross error ability of MPGAIB.

Parameters	Design value	Nearby of inflection points			Nearby of maximum subsidence points		
		Average value	AE	K/%	Average value	AE	K/%
q	1	1.005	0.005	0.515	1.012	0.012	1.208
P	0.7	0.630	0.070	10.021	0.726	0.026	3.690
b	0.3	0.296	0.004	1.333	0.295	0.005	1.509
θ	85	85.155	0.155	0.183	84.991	0.009	0.010
s1	45	45.430	0.430	0.955	45.650	0.650	1.445
s2	45	43.098	1.902	4.226	45.118	0.118	0.262
s3	45	45.513	0.513	1.140	43.719	1.281	2.846
s4	45	42.017	2.983	6.629	46.936	1.936	4.303
tanβ1	2	2.119	0.119	5.943	1.972	0.028	1.397
tanβ2	4	4.100	0.100	2.500	3.886	0.114	2.849

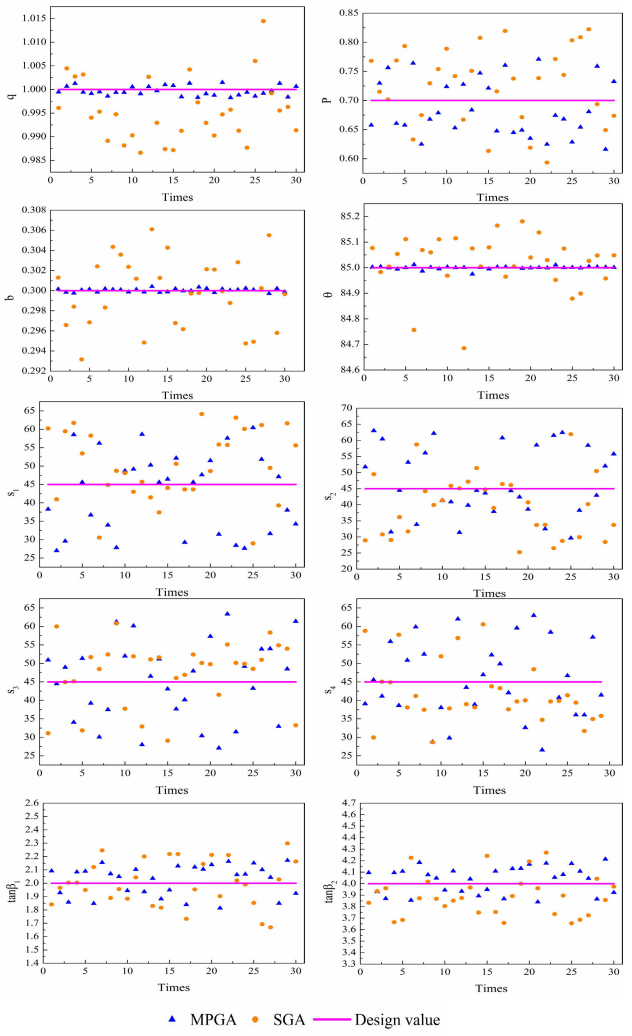

FIGURE 14. Comparison of fluctuation range of two methods.

ence on parameter inversion value, and the maximum relative error is 13.540%. The main reason is that the parameter tanβ1 is small, and its absolute error is only 0.271. Therefore, MPGAIB has a strong ability to anti-random errors. In complex terrain areas, it can appropriately reduce the accuracy requirements of surface movement monitoring, which has little impact on the accuracy of inversion parameters.

D. ANTI-GROSS ERROR ABILITY OF MPGAIB

The literature [22] pointed out that the error at the inflection point and the maximum subsidence point of the subsidence curve has the greatest impact on the parameter acquisition results. This article is to verify the anti-gross ability of the model, add 200 mm error at the maximum subsidence value and the inflection point, and then participate inversion, the inversion results are shown in Table.4.

It can be seen from Table.4 that after setting the gross error at the inflection point and maximum subsidence, the K of each parameter calculation value increases, and the K is between 0.010∼10.021%, which shows that the gross error has a certain influence on the inversion result. But the AE is small, which shows that the MPGAIB model has a better ability to anti-gross errors.

IV. ENGINEERING EXAMPLE

To verify the correctness of the IB, Taking 1222 (1) working face of Zhujidong mine in the Huainan mining area as an example. At the same time, the PIM prediction model, the Boltzmann function model, and the IB model were used for fitting and comparison. The methods of calculating parameters are all based on MPGA algorithm (The parameter settings are shown in Table 1.).

A. EXPERIMENT AREA AND REAL DATA

1222(1) working face has an average mining height of 1.9 m. The mining size is 805m×230 m. The average mining speed is 3.7 m/d and the coal seam inclination angle is 3°.It is a near-horizontal coal seam with an average mining depth of 945 m. The average thickness of the unconsolidated layer is 321 m. The working face adopts the comprehensive mechanized coal mining technology, and the full caving method is used for roof management. The 1222 (1) working face stopping time is from March 25, 2017 to October 26, 2017, which lasted 215 days. The layout of the monitoring points above the working face is shown in Fig.15.

The surface movement observation time of 1222(1) working face is from March 19, 2017 to September 18, 2018, and the observation work lasts 548 days, including connection measurement and the first comprehensive observation, two patrol surveys, one daily observation and 22 comprehensive

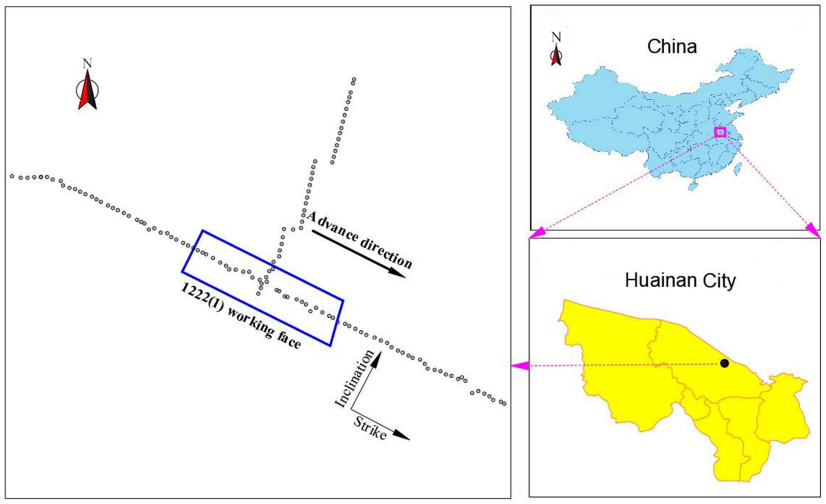

FIGURE 15. The chart of observation line layout in 1222(1) working face.

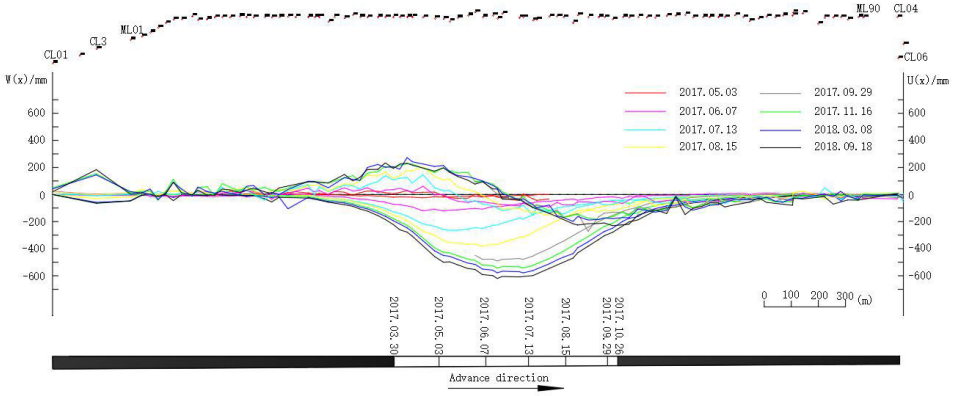

FIGURE 16. Subsidence and horizontal movement curves of 1414(1) working face along strike.

observation in the mining process. GNSS-RTK technology is used for plane observation, and digital level is used for elevation measurement according to the requirements of 3-class leveling. The values of partial subsidence and horizontal movement are shown in Fig.16 and Fig.17.

B. DATA PROCESSING AND ANALYSIS

The observed subsidence and horizontal movement values of 1222 (1) working face in the last period are brought into the MPGAIB model constructed in this paper. The fitting results are shown in Fig.18 and Fig.19. For comparison, the IB model constructed in this paper is compared with the PIM model and the Boltzmann model to calculate the total fitting error, subsidence boundary fitting error, and horizontal movement boundary fitting error of the three predicted models. The error index is Root Mean Squared Error (RMSE) and Mean Absolute Error (MAE), the results are shown in Table.5.

It can be seen from Fig.17 and Fig.18 that compared to the PIM model and the Boltzmann model, the IB model has a better fit for the subsidence and horizontal movement

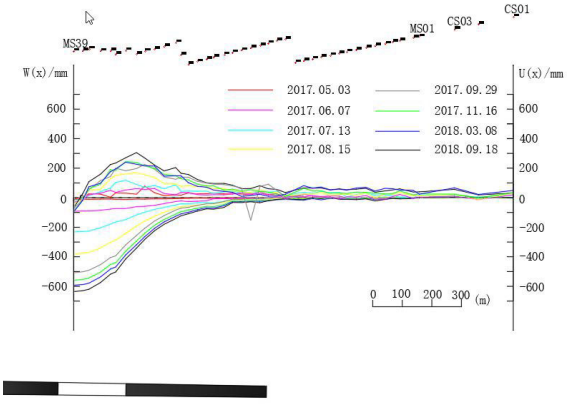

FIGURE 17. Subsidence and horizontal movement curves of 1414(1) working face along inclination.

values at the boundary. It can be seen from Table.5 that the RMSE and MAE values of the IB model are smaller than the Boltzmann model and the PIM model regardless of the fitting error of all points or the points at the boundary, indicating

TABLE 5. Parameters of different prediction models.

Models	Parameters	误差	All points /mm	Subsidence boundary /mm	Horizontal movement boundary /mm
PIM	q=0.84, tanβ=1.88, b=0.39, θ=81.8, s_1=18.4, s_2=17.0, s_3=-12.4, s_4=-11.3	RMSE	54.5	29.7	41.5
		MAE	28.4	18.8	36.0
Boltzmann	q=0.90, tanβ=1.80, b=0.38, θ=81, s_1=19.3, s_2=16.8, s_3=-7.6, s_4=-7.1	RMSE	49.2	29.1	37.3
		MAE	26.0	17.1	31.5
IB	q=0.93, P=0.12, b=0.41, θ=82.1, s_1=23.0, s_2=18.9, s_3=-6.9, s_4=-6.4, tanβ_1=1.6, tanβ_2=3.01	RMSE	46.7	27.6	34.8
		MAE	23.9	14.4	28.3

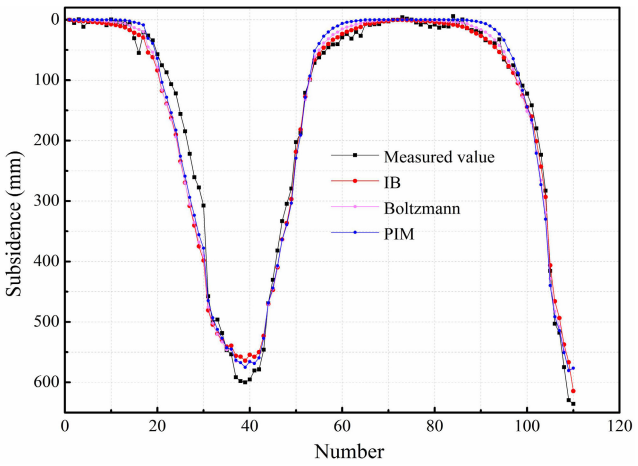

FIGURE 18. Comparison chart of fitted subsidence value and measured subsidence value of 1222(1) working face.

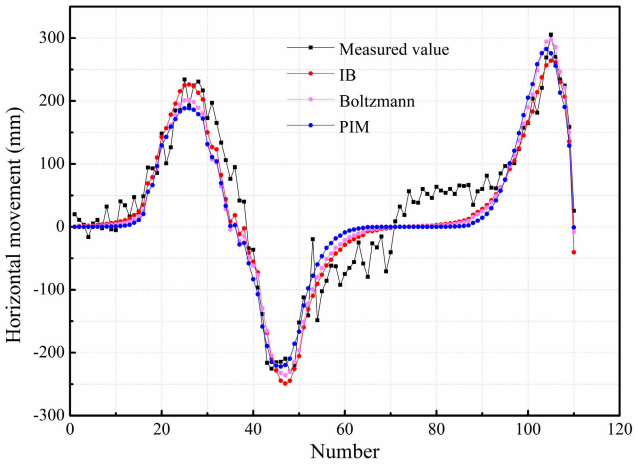

FIGURE 19. Comparison chart of fitted horizontal movement value and measured horizontal movement value of 1222(1) working face.

That the IB model has the highest accuracy, the Boltzmann model takes the second place and the PIM model has the worst accuracy.

V. DISCUSSIONS

A. GLOBAL SENSITIVITY ANALYSIS OF IB MODEL

Sensitivity analysis is often used to study and analyze the sensitivity of state or output changes of a system (or a model) to changes of system parameters or surrounding conditions. In the optimization method, sensitivity analysis is often used to study the stability of the optimal solution when the original data are inaccurate or unstable [23]. It can also determine which parameters have a greater impact on the system or model. In this paper, orthogonal design statistical analysis was used to analyze the sensitivity of parameters in the IB, aiming to find out the importance of the parameters that affect the prediction results, and provide an important basis for the selection of initial parameters and the application of the model in the process of parameter calculation.

TABLE 6. Factors scheme in orthogonal experiment.

Type	1	2	3	4	5
q	0.8	0.9	1.0	1.1	1.2
P	0.5	0.6	0.7	0.8	0.6
s/H	0.03	0.06	0.09	0.11	0.13
tanβ_1	1.6	1.8	2	2.2	2.4
tanβ_2	3.6	3.8	4	4.2	4.4

In this paper, taking the simulated working face established in Section III as an example, the orthogonal parameter table is set according to the predicted parameter range of the simulated working face, and each group of parameters is brought into the model for prediction. The predicted results are compared with the measured values, and then the range analysis method is used to analyze the influence of parameters on the results.

1) CALCULATION SCHEME OF THE MODEL

According to the inversion process of the actual data, the mining influence propagation angle has little influence on the results. The horizontal movement coefficient b is related to horizontal movement. Therefore, the two parameters remained unchanged in the experiment, and the factors q, P, s/H, tanβ_1, tanβ_2 were selected as five factors of the orthogonal experiment. Each factor has five levels, as shown in Table.6.

2) ANALYSIS OF EXPERIMENTAL RESULTS

According to Table.6, 25 calculation models can be established. The mean square error of subsidence value fitting can be selected as index results. The orthogonal experimental results are shown in Table.7.

TABLE 7. Orthogonal experimental results of surface subsidence.

No.	q	P	s/H	$\tan\beta_1$	$\tan\beta_1$	Mean square error of fitting/mm
1	0.8	0.5	0.03	1.6	3.6	330.58
2	0.8	0.6	0.06	1.8	3.8	256.48
3	0.8	0.7	0.09	2	4	274.92
4	0.8	0.8	0.12	2.2	4.2	425.20
5	0.8	0.9	0.15	2.4	4.4	675.91
6	0.9	0.5	0.06	2	4.2	160.86
7	0.9	0.6	0.09	2.2	4.4	136.69
8	0.9	0.7	0.12	2.4	3.6	366.21
9	0.9	0.8	0.15	1.6	3.8	648.36
10	0.9	0.9	0.03	1.8	4	323.85
11	1	0.5	0.09	2.4	3.8	54.57
12	1	0.6	0.12	1.6	4	357.52
13	1	0.7	0.15	1.8	4.2	585.35
14	1	0.8	0.03	2	4.4	435.77
15	1	0.9	0.06	2.2	3.6	245.99
16	1.1	0.5	0.12	1.8	4.4	263.11
17	1.1	0.6	0.15	2	3.6	534.25
18	1.1	0.7	0.03	2.2	3.8	531.33
19	1.1	0.8	0.06	2.4	4	398.09
20	1.1	0.9	0.09	1.6	4.2	208.96
21	1.2	0.5	0.15	2.2	4	468.57
22	1.2	0.6	0.03	2.4	4.2	688.48
23	1.2	0.7	0.06	1.6	4.4	421.94
24	1.2	0.8	0.09	1.8	3.6	226.79
25	1.2	0.9	0.12	2	3.8	172.14

TABLE 8. Direct analysis of mean square errors in subsidence fitting.

Parameter	q	P	s/H	$\tan\beta_1$	$\tan\beta_2$
Average 1	392.6	255.5	462.0	393.5	340.8
Average 2	327.2	394.7	296.7	331.1	332.6
Average 3	335.8	436.0	180.4	315.6	364.6
Average 4	387.2	426.8	316.8	361.6	413.8
Average 5	395.6	325.4	582.5	436.7	386.7
Range	68.4	180.4	402.1	121.1	81.2

By using the method of range analysis, we can get the change rule of each factor with the index from the statistical point of view. The mean value and range of each factor at each level can be calculated from Table.7, as shown in Table.8.

The greater the range, the greater the influence of this factor on the results. In IB, the ranges of the fitting mean square errors of parameters q, P, s/H, $\tan\beta_1$ and $\tan\beta_2$ are 68.4, 180.4, 402.1, 121.1 and 81.2, respectively. This shows that the biggest factor affecting the predicted subsidence is s/H, and the smallest factor is q. The acquisition of sensitivity is of great significance for the selection of initial parameters of the IB.

B. RELATIONSHIP BETWEEN IB MODEL PARAMETERS AND GEOLOGICAL MINING CONDITIONS

How to obtain the model parameters before mining is of great significance to the design of the working face, the observation station and the protective measures for the buildings. In this paper, the relationships between the model parameters and the geological and mining conditions were studied based on the measured data under the thick alluvium in the Huainan mining area. The established multiple linear regression model is shown in Equation (26).

$$P_a = \beta_0 + \beta_1 V_1 + \cdots + \beta_m V_m \tag{26}$$

where β_0, β_1,..., β_{m} are the regression coefficients and V_0, $V_1, \ldots, V_{\mathrm{m}}$ are the geological and mining condition.

On the basis of sorting out the surface observation stations of multiple working faces, the MPGA was used to obtain the parameters of the IB model. The inversion results are shown in Table.9.

The geological and mining conditions collected in this paper include the mining thickness m, mining depth h, unconsolidated layer thickness h_{s}, coal seam dip angle α, dip mining degree D_1/H (the ratio of inclination length to mining depth), and working face advance speed v. Due to the wide fluctuation range of offset of the inflection point, $0.1H$ was taken for Huainan mining area without considering the regression formula temporarily. The relationships between the above parameters and geological and mining conditions were established by using linear regression method as shown in Table.10.

The size of the fitting coefficient represents the influence of the independent variable on the dependent variable

TABLE 9. Fitting parameters.

No.	Prediction parameters									
	q	P	b	θ	s_1	s_2	s_3	s_4	$\tan\beta_1$	$\tan\beta_2$
1222(1)	0.83	0.64	0.43	87	10.8	-2.8	16.2	-12.5	0.85	2.50
1613(1)	1.01	0.63	0.31	87	-19.5	8.4	65	41.6	0.90	2.70
1312(1)	1.32	0.30	0.34	89	-0.83	-18.7	100.0	99.9	1.12	4.99
2111(3)	0.86	0.42	0.32	82	2.40	-29.7	44.5	49.8	1.10	3.80
121301	1.09	0.66	0.35	80	-44.9	-40.0	56.5	49.4	1.25	3.62
1414(1)	0.98	0.49	0.4	80	-31.0	-25.2	46.5	29.9	1.27	3.91
1111(1)	0.69	0.19	0.41	90	19.5	-4.0	-29.8	-28.3	0.76	2.81
1252(1)	0.73	0.45	0.33	86	26.7	8.3	49.1	28.9	0.95	2.91
111303	1.30	0.69	0.49	86	38.4	10.9	11.8	18.3	1.02	2.75

TABLE 10. Regression fitting coefficients.

	m	a	h_s/H	D_1/H	v	β_0	R^2
q	-0.138	0.035	1.41	0.085	-0.07	0.521	0.98
P	-0.188	0.033	1.133	-0.181	-0.078	0.835	0.96
b	-0.073	0.013	0.580	-0.671	-0.076	0.787	0.98
θ	-0.697	-0.524	10.567	-8.421	-0.924	93.598	0.87
$\tan\beta_1$	0.044	0.017	-0.299	0.779	0.096	0.209	0.88
$\tan\beta_2$	0.433	-0.078	-0.958	3.513	0.573	-0.698	0.89

parameters, and the sign represents the influence direction. According to the above formulas, the required parameters can be obtained before mining.

C. RELATIONSHIP BETWEEN IB PREDICTION PARAMETERS AND PIM PREDICTION PARAMETERS

PIM is a widely used surface prediction method. The parameters in PIM, such as subsidence coefficient (q_{PIM}), horizontal movement coefficient (b_{PIM}), propagation angle of mining influence (θ_{PIM}), tangent of main influence angle ($\tan\beta_{\mathrm{PIM}}$) and offset of inflection point ($s_{1\mathrm{PIM}}$, $s_{2\mathrm{PIM}}$, $s_{3\mathrm{PIM}}$, $s_{4\mathrm{PIM}}$), are the same as those of IB model, but the parameters have certain changes. Therefore, through establishing the mathematical relationship between IB model parameters and PIM model parameters, the conversion model between them is established It is of great significance to make full use of the parameters of PIM of existing working face. Table.9 shows the calculated parameters of PIM for some working faces.

(1) The relationship between q and q_{PIM}

By establishing the linear relationship between q and q_{PIM}, as shown in Fig.20, the regression relationship is shown in Equation (27):

$$q = 0.9581q_{\mathrm{PIM}} + 0.1408 \tag{27}$$

The fitting results show that q increases with the increase of q_{PIM}.

(2) The relationship between b and b_{PIM}

By establishing the linear relationship between b and b_{PIM}, as shown in Fig.21, the regression relationship is shown in Equation (28):

$$b = 1.0739b_{\mathrm{PIM}} + 0.0073 \tag{28}$$

The fitting results show that b increases with the increase of b_{PIM}.

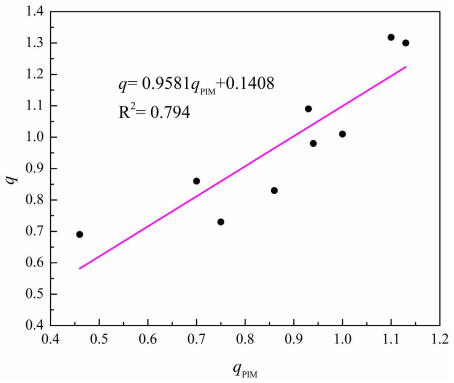

FIGURE 20. The relationship between q and q_{PIM}.

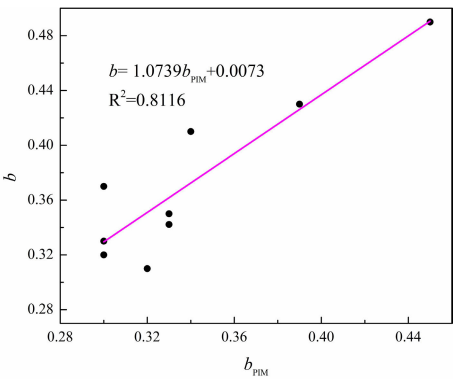

FIGURE 21. The relationship between b and b_{PIM}.

(3) The relationship between $\tan\beta_1$ and $\tan\beta_{\mathrm{PIM}}$

By establishing the linear relationship between $\tan\beta_1$ and $\tan\beta_{\mathrm{PIM}}$, as shown in Fig.22, the regression relationship is shown in Equation (29),

$$\tan\beta_1 = 0.6767\tan\beta_{\mathrm{PIM}} - 0.3327 \tag{29}$$

The fitting results show that $\tan\beta_1$ increases with the increase of $\tan\beta_{\mathrm{PIM}}$.

(4) The relationship between $\tan\beta_2$ and $\tan\beta_{\mathrm{PIM}}$

By establishing the linear relationship between $\tan\beta_2$ and $\tan\beta_{\mathrm{PIM}}$, as shown in Fig.23, the regression relationship is shown in Equation (30),

$$\tan\beta_2 = 2.3477\tan\beta_{\mathrm{PIM}}\text{-}1.4305 \tag{30}$$

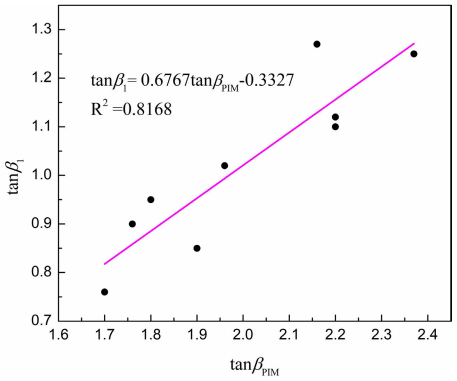

FIGURE 22. The relationship between $\tan\beta_1$ and $\tan\beta_{PIM}$.

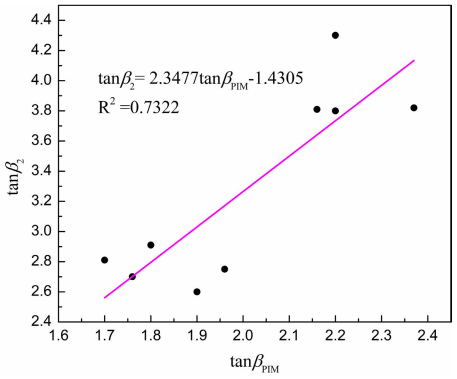

FIGURE 23. The relationship between $\tan\beta 2$ and $\tan\beta_{PIM}$.

The fitting results show that $\tan\beta_2$ increases with the increase of $\tan\beta_{PIM}$.

If the parameters of PIM in this mining area are known, the parameters of IB model can be determined by (27) ∼ (30), and IB model is used for prediction, so as to make up for the shortcomings of the traditional PIM model with too fast edge convergence and improve the prediction accuracy.

VI. CONCLUSION

The prediction parameters inversion of surface subsidence in coal mining is a hot spot and difficulty in deformation monitoring data processing.

In order to solve the problem of slow convergence of surface boundary in thick unconsolidated layer mining area, a new surface prediction model is proposed in this paper, and MPGA algorithm is introduced to solve the model parameters. The main conclusions of this paper are as follows:

(1) A new model IB was proposed. According to the superposition principle, the formulas of predicting the main section along the strike and inclination as well as an any point were given.

(2) The MPGA algorithm was introduced into the process of model parameter solving, and the MPGAIB model was constructed. The simulation experiment results show that the MPGAIB model is stable and has strong resistance to random errors and gross errors. The MPGAIB model is applied to 1222 (1) working surface, the result shows: the mean square errors of the total fitting, subsidence boundary fitting and horizontal movement boundary fitting were 46.7 mm, 27.6 mm and 34.8 mm, and the horizontal movement boundary fitting mean square error was 55.1 mm. The fitting accuracy of the IB model was higher than the Boltzmann model and the PIM model.

(3) The orthogonal design algorithm is used to discuss the influence of the model parameters on the predicted results. The calculated error ranges of the parameters q, P, s/H, $\tan\beta_1$, $\tan\beta_2$ are 68.4, 180.4, 402.1, 121.1, 81.2, respectively. This shows that the largest factor affecting the predicted result of subsidence was s/H, and the smallest factor was q. The relationship between the predicted parameters of the IB model and the parameters of the PIM model and the geological mining conditions is analyzed and discussed, which provides a basis for the solution of the model parameters.

REFERENCES

[1] I. Contrucci, C. Balland, J. Kinscher, M. Bennani, P. Bigarré, and P. Bernard, "Aseismic mining subsidence in an abandoned mine: Influence factors and consequences for post-mining risk management," *Pure Appl. Geophys.*, vol. 176, no. 2, pp. 801–825, Feb. 2019.

[2] M. Zheng, H. Zhang, K. Deng, S. Du, and L. Wang, "Analysis of pre-and post-mine closure surface deformations in western Xuzhou coalfield from 2006 to 2018," *IEEE Access*, vol. 7, pp. 124158–124172, 2019.

[3] Z. Yang, Z. Li, J. Zhu, A. Preusse, J. Hu, G. Feng, Y. Wang, and M. Papst, "An InSAR-based temporal probability integral method and its application for predicting mining-induced dynamic deformations and assessing progressive damage to surface buildings," *IEEE J. Sel. Topics Appl. Earth Observ. Remote Sens.*, vol. 11, no. 2, pp. 472–484, Feb. 2018.

[4] E. F. Salmi, M. Karakus, and M. Nazem, "Assessing the effects of rock mass gradual deterioration on the long-term stability of abandoned mine workings and the mechanisms of post-mining subsidence—A case study of castle fields mine," *Tunnelling Underground Space Technol.*, vol. 88, pp. 169–185, Jun. 2019.

[5] C. Liu, H. Li, and H. Mitri, "Effect of strata conditions on shield pressure and surface subsidence at a longwall top coal caving working face," *Rock Mech. Rock Eng.*, vol. 52, no. 5, pp. 1523–1537, May 2019.

[6] S. Zhu, Y. Feng, and F. Jiang, "Determination of abutment pressure in coal mines with extremely thick alluvium stratum: A typical kind of rockburst mines in China," *Rock Mech. Rock Eng.*, vol. 49, no. 5, pp. 1943–1952, May 2016.

[7] D. H. Li, *Study on Strip Mining Technology Under Thick Loose Layer*. Beijing, China: Science and Technology of China Press, 2008, pp. 14–35.

[8] D. Zhou, K. Wu, and L. Li, "Combined prediction model for mining subsidence in coal mining areas covered with thick alluvial soil layer," *Bull. Eng. Geol. Environ.*, vol. 77, no. 1, pp. 283–304, Feb. 2018.

[9] N. Wang, K. Wu, and S. K. An, "Model for mining subsidence prediction based on Boltzmann function," *J. China Coal Soc.*, vol. 38, no. 8, pp. 1352–1356, Aug. 2013.

[10] X. M. Cui, *Dynamic Monitoring and Mechanical Analysis of Large Deformation of Subsidence*. Beijing, China: China Coal Industry Publishing House, 2004, pp. 1–10.

[11] S. S. Peng, *Surface Subsidence Engineering*. Littleton, CO, USA: The Society for Mining, Metallurgy, and Exploration, 1992, pp. 31–40.

[12] J. Zuo, Y. Sun, and M. Qian, "Movement mechanism and analogous hyperbola model of overlying strata with thick alluvium," *J. China Coal Soc.*, vol. 42, no. 6, pp. 1372–1379, Jun. 2017.

[13] H. S. Zhang and W. Gu, "Establishment and application of typical curve method for Longkou soft rock coal-mining area in Shandong province," *Contrib. Geol. Mineral Resour. Research.*, vol. 29, no. 1, pp. 84–90, Apr. 2014.

[14] Y. C. Liu and H. Y. Dai, "Hyperbolic function model for predicting the main section surface deformation proximate horizontal coal seam underground longwall mining," *J. China Univ. Mining Technol.*, vol. 48, no. 3, pp. 676–681, May 2019.

[15] L. Wang, T. Wei, N. Li, S.-S. Chi, C. Jiang, and S.-Y. Fang, "Research on probability integration parameter inversion of mining-induced surface subsidence based on quantum annealing," *Environ. Earth Sci.*, vol. 77, no. 21, p. 740, Nov. 2018.
[16] Z. Chang, J. Wang, M. Chen, Z. Ao, and Q. Yao, "A novel ground surface subsidence prediction model for sub-critical mining in the geological condition of a thick alluvium layer," *Frontiers Earth Sci.*, vol. 9, no. 2, pp. 330–341, Jun. 2015.
[17] T. Unlu, H. Akcin, and O. Yilmaz, "An integrated approach for the prediction of subsidence for coal mining basins," *Eng. Geol.*, vol. 166, pp. 186–203, Nov. 2013.
[18] H. Li, J. Zha, and G. Guo, "A new dynamic prediction method for surface subsidence based on numerical model parameter sensitivity," *J. Cleaner Prod.*, vol. 233, pp. 1418–1424, Oct. 2019.
[19] W. Yang and X. Xia, "Prediction of mining subsidence under thin bedrocks and thick unconsolidated layers based on field measurement and artificial neural networks," *Comput. Geosci.*, vol. 52, pp. 199–203, Mar. 2013.
[20] R. D. Lokhande, V. M. S. R. Murthy, and K. B. Singh, "Predictive models for pot-hole depth in underground coal mining—Some indian experiences," *Arabian J. Geosci.*, vol. 7, no. 11, pp. 4697–4705, Nov. 2014.
[21] K. Wu and Z. Jin, "Application of time series analysis in prediction of mining subsidence dynamic parameters," *J. China Univ. Mining Technol.*, vol. 29, no. 4, pp. 413–415, Apr. 2000.
[22] J. Zha, W. Feng, and X. Zhu, "Research on parameters inversion in probability integral method by genetic algorithm," *J. Mining Saf. Eng.*, vol. 28, no. 4, pp. 655–659, Aug. 2011.
[23] E. Pisoni, D. Albrecht, T. A. Mara, R. Rosati, S. Tarantola, and P. Thunis, "Application of uncertainty and sensitivity analysis to the air quality SHERPA modelling tool," *Atmos. Environ.*, vol. 183, pp. 84–93, Jun. 2018.

SHENSHEN CHI was born in Anhui, China, in 1992. He received the B.S. and M.S. degrees in geomatics from the Anhui University of Science and Technology, Huainan, Anhui, China, in 2015 and 2018, respectively, where he is currently pursuing the Ph.D. degree. His research interests include RS/GIS fusion technology, environmental and disaster air-space-earth collaborative monitoring theory and technology, and mining subsidence deformation monitoring and mechanism analysis.

LEI WANG received the Ph.D. degree from the School of Environment and Spatial Informatics, China University of Mining and Technology, China. He is currently an Associate Professor with the School of Geomatics, Anhui University of Science and Technology, China. He is also the Secretary of the Coal Industry Engineering Research Center for collaborative monitoring of environment and disasters and the Key Laboratory of Collaborative Monitoring and Early Warning of Mining Disasters, Anhui University. His present research interests include InSAR deformation monitoring and data processing and evaluation theory and control technology of mining ground stability in mining area.

XUEXIANG YU received the Ph.D. degree from the School of Geodesy and Geomatics, Wuhan University, China. He is currently a Professor and the Dean with the School of Geomatics, Anhui University of Science and Technology, China. His present research interests include GNSS/GIS integration, deformation monitoring automation, disaster monitoring and prediction, software engineering, and mine spatial information technology.

XINJIAN FANG received the Ph.D. degree from the School of Earth and Environment, Anhui University of Science and Technology, China. He is currently a Lecturer with the School of Geomatics, Anhui University of Science and Technology. His present research interests include GNSS precision positioning technology, GNSS/TLS integration theory and method, multi-source monitoring, and mechanism analysis of deformation disasters.

CHUANG JIANG was born in Anhui, China, in 1993. He received the B.S. and M.S. degrees in geomatics from the Anhui University of Science and Technology, Huainan, Anhui, China, in 2016 and 2019, respectively, where he is currently pursuing the Ph.D. degree. His research interests include mining subsidence and strata control, three under mining, and deformation monitoring and prediction.